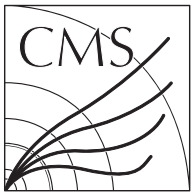

Analysis of Central Diffraction with the CMS-TOTEM Precision Proton Spectrometer

Ash Samra[1]

Supervisors: Jonathan J. Hollar [2], Michael Pitt[3]

[1]*University of Victoria, Department of Physics and Astronomy*
[2]*LIP Lisbon*
[3]*CERN*

22 August 2025

Abstract

We present an analysis of central diffractive events in proton–proton collisions using the CMS-TOTEM Precision Proton Spectrometer (PPS). By tagging protons and reconstructing vertex positions via timing detectors, we explore a class of pomeron-mediated interactions in a non-perturbative QCD regime. We study kinematic distributions in data and simulation, applying event selection, timing correlations, event mixing, and sideband subtraction to estimate and separate background. We present one of the first cross-section measurements of central diffraction at LHC energies, providing new insights into a poorly modelled process.

As an addition to this primary project, we also detail the process of testing a proposed upgrade to the PPS timing detectors in the CERN Prévessin site test beam. In particular, we show how to automate data taking to characterise amplifiers used in the detector.

Contents

1 Introduction

Central diffraction in proton-proton collisions is process wherein two colliding protons irradiate photons or pomerons, resulting in a colour neutral exchange. The dissociative products interact forming some central system, X, resulting in a final state $pp \rightarrow pXp$ (Figure 1.1 [1]). Various possible models are used to describe central diffraction, each predicting different cross sections, however, until now, no measurement of this process has been performed at LHC energies. The aim of this project is to compare the measured distributions and cross section of central diffraction in data to different theoretical predictions, in particular considering the Schuler and Sjöstrand (SaS) and Appleby, Barlow, Molson, Serluca and Toader (ABMST) models[2].

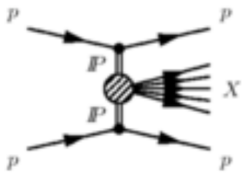

Figure 1.1: Feynman diagram of central diffraction.

Central diffraction is distinct from central *exclusive* diffraction in that the momentum of each respective photon or pomeron—equal to the fractional longitudinal momentum loss, $\xi = \frac{\Delta p}{p}$, of the associated proton—is not entirely transferred to the central system products. From an analysis perspective, this makes the measurement of central diffraction far more difficult as we can no longer easily associate central system properties to the outgoing proton momenta losses using the following relations without some corrective factor:

$$M_X = \sqrt{s}\sqrt{\xi_1 \xi_2} \tag{1.1}$$

$$Y_X = \frac{1}{2} ln \left(\frac{\xi_1}{\xi_2} \right) \tag{1.2}$$

One of the primary physics cases of the CMS-TOTEM Precision Proton Spectrometer (PPS) is in tagging outgoing protons to identify central diffractive events. The PPS detector consists of two arms on either side of the central CMS detector, each roughly 200 metres away. Identical layers of tracking and timing detectors are housed in movable cylindrical vessels called Roman Pots (RPs) on either side (see Figure 1.2 [3]), measuring the x and y position and time of arrival (ToA) of incident protons. Currently, the tracking detectors uses 3D pixel detectors and the timing detectors use double diamond detectors[4].

The timing detectors of PPS allow us to reconstruct the original z position offset from the interaction point at the centre of the central CMS detector by measuring the difference in ToA of the final state protons on each side. Assuming the protons travel at the speed of light, and allowing t_F and t_B to be the ToA of the forward and backward protons respectively, the z position of the vertex (that is, the location where the collision occurred) is given by:

$$z_{vtx} = \frac{c}{2}(t_F - t_B) \tag{1.3}$$

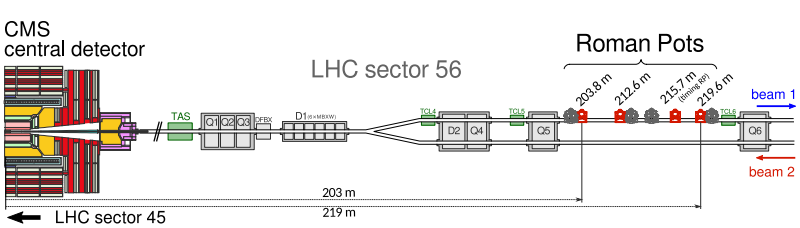

(a) Central CMS detector and one arm of PPS.

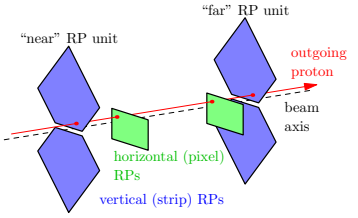

(b) Roman pot structure: one layer of tracking detector, two layers of timing detectors, and one layer of tracking detector.

Figure 1.2: Diagram of the PPS detector and RPs.

The central detector also measures the z position of the vertex for each event. The reconstructed and measured values can therefore be compared; the two positions will be highly correlated for central diffractive events.

In our measurements, proton pileup is the predominant background. These protons do not necessarily originate from the same vertex as the central diffractive protons. Indeed, they come from random positions, thus we expect the timing measurements to be uncorrelated to the measured vertex position. By measuring the correlation between the measured and reconstructed position, we can estimate the efficiency of our signal (central diffractive) event selection.

The primary focus of this report is the analysis of central diffraction, as this was the bulk of this project. The secondary focus in chapter 5 is a shorter, hands-on portion of the project where we tested a proposed High Luminosity LHC upgrade of the PPS timing detector in the test beam at the CERN Prévessin site.

2 Data and Monte Carlo Samples

The data sample used in this analysis was from CMS Run 319488, collected with the `HLT_ZeroBias` trigger, 13 TeV of collision energy, and an integrated luminosity with corrections for trigger prescales of 0.899 nb^{-1}. The mean pileup of this sample is 1.

The Monte Carlo (MC) signal samples are generated using PYTHIA8 at 13 TeV, with filter cuts of m > 250 GeV and proton $\xi > 0.02$, and zero pileup. For the SaS MC sample, a total of 7787 events were simulated, with a cross section of 0.092 mb. The ABMST MC sample simulated 99893 events and had a cross section of 0.0224 mb.

2.1 Event Selection

In order to select signal events we apply certain baseline selection cuts informed by the expected signature and final state of central diffractive events. A central diffractive event is composed of two protons,

one vertex, and two timing tracks, all of which pass some criteria of "good" objects. A good proton must be measured in all the RPs and have timing information; an event is selected if we have only two such protons and they are from opposite arms. A good vertex must be properly reconstructed by the detector, not assigned the default z position value of the beam spot location; we select events having only one such vertex. Finally, we select events with only two timing tracks, both being from separate arms.

As we do not have a priori knowledge of the signal distribution, initially, a heuristic approach was taken to event selection: cuts were applied and the quality of a selection was determined by how well the timing was correlated to position (Figure 2.1). However, we were able to use event-mixing (section 3.1) to characterize the background distributions by simulating the uncorrelated background resulting from pileup. The shape of the background distributions derived from these new event-mixing samples was compared to the data and Monte Carlo to inform selection criteria. The final cuts chosen for the working point are indicated in Table 2.1. Detailed comparisons of the distributions used to inform selection cuts are shown in Appendix A; this also includes a cut flow table showing the effect of each cut. The final number of passing events is summarized in Table 2.2.

We use the correlation of proton timing and measured vertex z position to quantify how well these selection cuts select signal events. Signal events should fall within the acceptance region defined by the diagonal band across the time correlation plots. The width of this band corresponds to the timing and position resolution. For signal and background samples, it is found by fitting the difference between the measured and reconstructed position (Equation 1.3) with a Gaussian, and taking the standard deviation as the resolution. For data however, since it is the sum of background and signal, we assume a sum of two Gaussians as the distribution and fit this, taking the signal standard deviation as the resolution. This is illustrated for the final selection cuts in Figure 2.2.

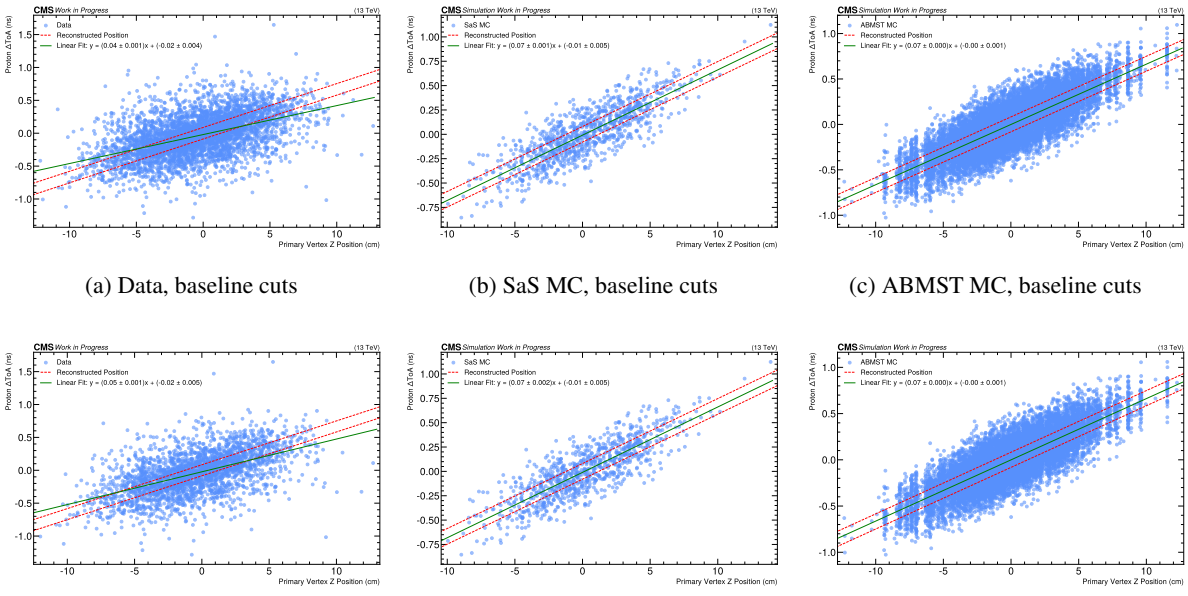

(a) Data, baseline cuts (b) SaS MC, baseline cuts (c) ABMST MC, baseline cuts

(d) Data, final cuts (e) SaS MC, final cuts (f) ABMST MC, final cuts

Figure 2.1: Data and MC timing correlations with baseline and final selection cuts.

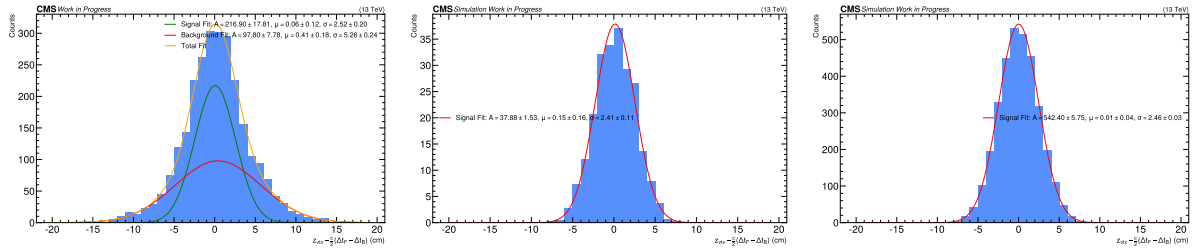

(a) Data, final cuts (b) SaS MC, final cuts (c) ABMST MC, final cuts

Figure 2.2: Fits of difference between measured and reconstructed position in data and MC for samples after final selection cuts.

Variable	Cut
Proton θ_x	absolute value <= 250 μrad
Proton θ_y	absolute value <= 500 μrad
Number of tracks in vertex	<= 20
Timing resolution of timing track	<= 0.20
Forward calorimeter energy deposit (+z side)	<= 200 GeV
Forward calorimeter energy deposit (-z side)	<= 200 GeV
Number of hits in forward calorimeter (+z side)	<= 20
Number of hits in forward calorimeter (-z side)	<= 20

Table 2.1: Final selection cuts.

	Data	SaS MC	ABMST MC	Event mixing
Events passing after final cuts	2661	920	13337	559
Total events	106324	7787	99893	100000
Fractional events passing	0.025	0.118	0.134	0.006

Table 2.2: Number and fraction of events passing after applying final cuts.

2.2 Efficiency Corrections

Monte Carlo models do not always reproduce detector inefficiencies, resulting in an overestimation of measured events in simulation. We must therefore use data-driven efficiency corrections to account for this in the MC samples.

Proton Efficiency

The efficiency of reconstructing a proton depends on the detector arm and the proton's ξ (as shown in Figure 2.3). These values are centrally measured for all CMS analyses using protons[5]. Each proton is assigned a weight depending on its ξ value. As each event is comprised of two protons, and assuming the efficiency of both protons are uncorrelated, the total weight of a given event is the product of the two proton weights.

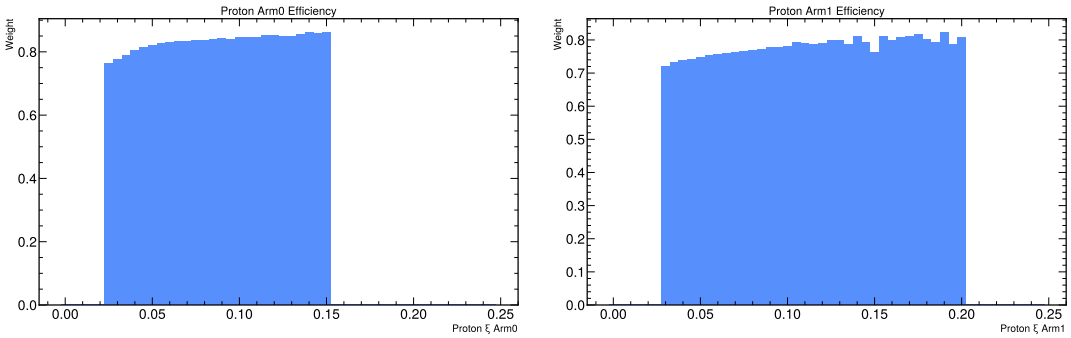

(a) Arm 0 Proton ξ Efficiency Histogram

(b) Arm 1 Proton ξ Efficiency Histogram

Figure 2.3: Proton reconstruction efficiencies in bins of proton ξ.

Vertex Efficiency

The vertex efficiency is defined as the probability of an event containing only one vertex. This is calculated as $\frac{\text{number of events with one vertex}}{\text{total number of events}} = 0.3988$. Figure 2.4 illustrates the distribution used to calculate this value.

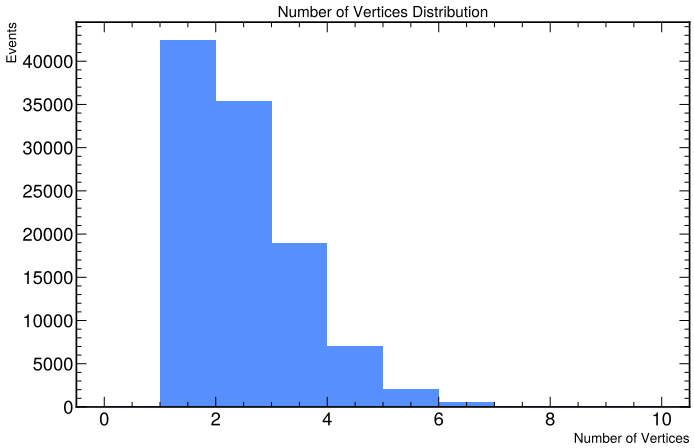

Figure 2.4: Number of vertices per event.

The total efficiency per event is the product of both the proton and vertex efficiency. This weight is applied to all the MC events; the sum of weights then gives the total number of signal events predicted by the MC.

3 Analysis

The aim of this analysis was to compare the final cross-section of central diffraction and distributions of various quantities from data to the predictions from the different physics models. In general, MC will simulate a signal process, whereas the data is a combination of signal and background processes. Obtaining

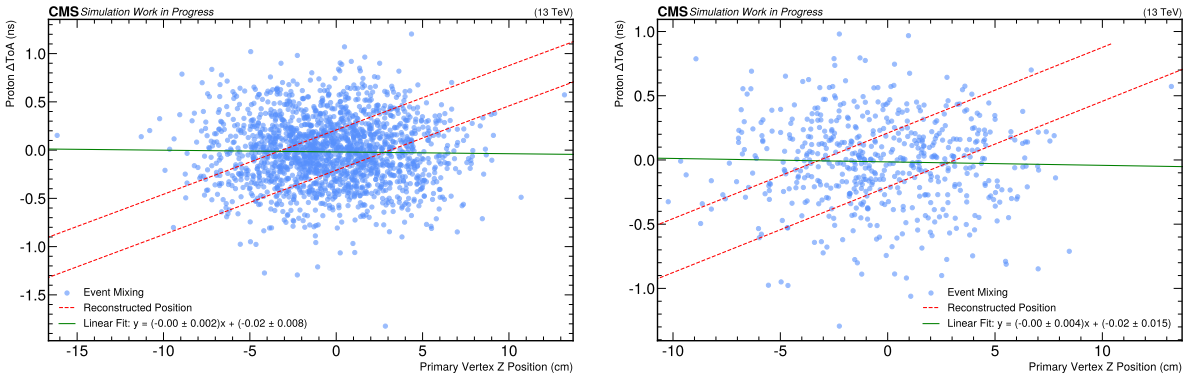

(a) Baseline cuts

(b) Final cuts

Figure 3.1: Event mixing timing correlation with baseline and final cuts

information about cross section and comparing signal event distributions requires us to measure with some confidence the total number of signal events and which events are signal within our data sample. The majority of the analysis focused on performing this measurement using various statistical methods.

Estimating the amount and shape of the background was important in informing selection cuts used to define the signal. Further, estimating the background distribution in the data was important to compare data to MC as the data should be the sum of signal and background. Background rejection is limited using a cuts-based selection method, hence we require other methods to estimate background distributions.

3.1 Event mixing

Event mixing was an useful technique to recreate the uncorrelated signature of the primary background, pileup protons. We chose, at random, six events from the data sample, not necessarily distinct. From each event we choose a different physics object and its associated properties. For example, from the first event we would take one proton and its associated properties (e.g. timing, arm, angle), from the second event we may take one vertex and its associated properties, and so on. For variables not directly associated with a physics object, the value is taken from the event associated with the first proton we choose. With this method, we create a new event composed of two protons, one vertex, and two timing track stubs. An object is chosen only if it passes certain threshold values: the protons must pass the `ProtonIsMultiRP` flag and the vertex must pass the `PrimVertexIsBS` flag. If the object from the event does not pass the baseline value, a different event is chosen at random. We created 100,000 events using this method.

By comparing the distributions of these events to both data and MC–as in Appendix A–we can see if any values are more common among background to rationalize further selection cuts. For example, looking at Figure A.9 and Figure A.8, larger values of these quantities seem to correspond to background processes. Thus, we make a cut on the maximum of these variables to be 200 GeV. Using the information we gained from event-mixing, we decided on the nominal working point for our selection cuts. Indeed, we can see by comparing the timing correlation and number of events passing after applying the baseline cuts as opposed to the final cuts (Figure 3.1), we lose a majority of the background.

3.2 Sideband Subtraction

Sideband subtraction is another method to estimate the background in the data [6]. A reference variable with an inferred background and signal distribution is chosen. In our analysis, the real and reconstructed position difference was chosen as the reference parameter. We fit the signal and background with the known distribution. For us, this a sum of two Gaussians:

$$f(x) = A_s e^{-\frac{(x-\mu_s)^2}{2\sigma_s^2}} + A_b e^{-\frac{(x-\mu_b)^2}{2\sigma_b^2}} \tag{3.1}$$

The unbinned data is fitted with a normalized Gaussian probability density function (PDF) using the RooFit algorithm which returns the event yields (N), means and standard deviations. The relative amplitudes for the signal and background Gaussians are then calculated using

$$A_i = \frac{N_i}{\int_{-\infty}^{\infty} exp\left(-\frac{(x-\mu_i)^2}{2\sigma_i^2}\right) dx} \tag{3.2}$$

The fit is performed with parametrizations determined by the fits of the same histogram from MC and event-mixing samples. The amplitudes are always kept as floating parameters, with the means and standard deviations being parameterized differently. This allows us to estimate a systematic uncertainty on the background.

The following four fits were performed: six free parameters ($A_s, \mu_s, \sigma_s, A_b, \mu_b, \sigma_b$); four free parameters with background constrained by fit; four free parameters with signal constrained by fit; two free parameters with both signal and background constrained by previous fits. The final two are performed with the signal constrained by the fit on both the SaS and ABMST MC. The constrained background fit is chosen as the working point and used to generate the nominal sideband-subtracted background distributions. We also get sideband-subtracted distributions from the remaining fits to estimate systematics. The fit algorithm using only signal parameterization did not converge, and thus these fits are excluded.

After fitting, we define signal (SR) and sideband (SBR) regions. The SR should contain majority signal events with some background, while the SBR is assumed to contain only signal events; we choose how to define these regions to fulfill these assumptions. The SR is defined as $1.5\sigma_s$ around μ_s, whereas the SBR is defined as between $2.5\sigma_s$ and $5\sigma_s$ around μ_s on either side. The sideband and signal region definitions as well as the fits can be seen in Figure 3.2.

From the data and region definitions, we select and separate events in the signal region and sideband region. SBR events are assumed to be entirely background, and we assume the shape we get from the sideband is the same as the background shape in the SR. Thus, we need only to scale the shape to the number of expected background events in the SR to get the background distribution in the SR. This scaling factor (SF) is calculated as

$$SF = \frac{N_{signal}}{N_{bkg}} = \frac{\int_{\mu_s-1.5\sigma_s}^{\mu_s+1.5\sigma_s} A_s exp\left(-\frac{(x-\mu_s)^2}{2\sigma_i^2}\right) dx}{\int_{\mu_s-5\sigma_s}^{\mu_s-2.5\sigma_s} A_b exp\left(-\frac{(x-\mu_b)^2}{2\sigma_i^2}\right) dx + \int_{\mu_s+2.5\sigma_s}^{\mu_s+5\sigma_s} A_b exp\left(-\frac{(x-\mu_b)^2}{2\sigma_i^2}\right) dx} \tag{3.3}$$

For each interest variable, we separately create histograms of the SR and SBR events (with the same binning – this is pre-defined for each variable). We apply the scaling factor to the SBR histogram and obtain the background distribution in the SR. This is done with each parametrization type for all interest variables. For a given parameter, for each bin, the average number of events in that bin is taken, and the difference between the nominal value and the mean is assigned as the systematic error to that bin.

4 Results

Our final results are the number of signal events and cross section measured from the data as they are compared to simulation. We also compare the various distributions of kinematic properties between data and MC.

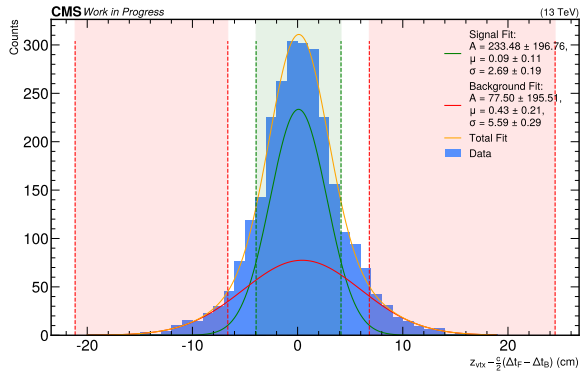

(a) Six free parameters

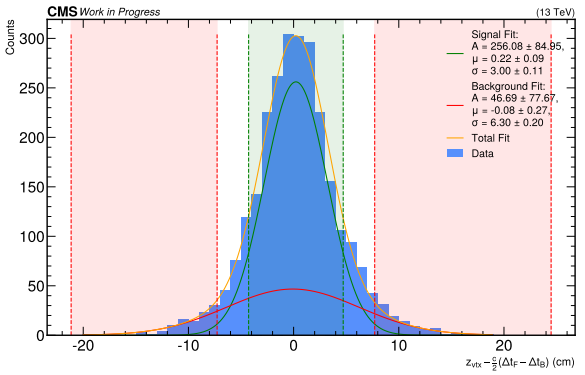

(b) Constrained background

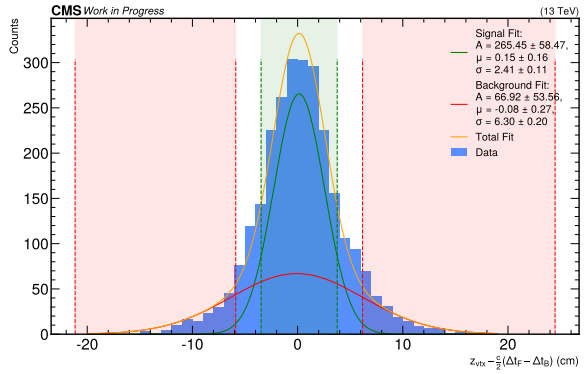

(c) Constrained signal (from SaS MC) and background

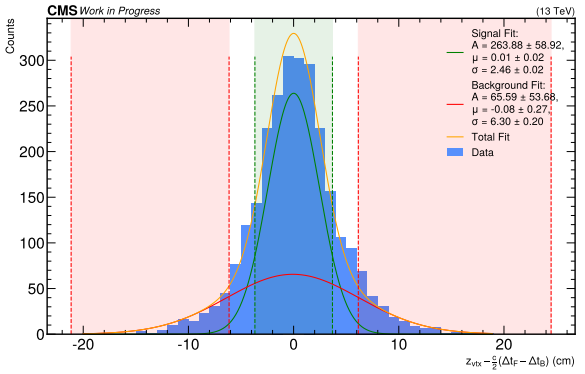

(d) Constrained signal (from ABMST MC) and background

Figure 3.2: Signal and sideband region definitions and fits for different parametrizations of measured and reconstructed position difference.

4.1 Event Yields

The total number of events from the MC is found from the sum of the weights of each event. We neglect uncertainty on the MC as the data uncertainty is assumed to be much larger. The total number of signal events in data is found from integrating the nominal signal fit in the signal region (Table 4.1). The statistical uncertainty is derived from the error on the fit, while the systematic uncertainty is found from integrating each of the other paramterizations and taking the largest difference between these and the nominal to be the uncertainty.

	n_{events} Signal
Data	1668 ± 62 (stat) ± 187 (syst)
SaS MC	2432
ABMST MC	674

Table 4.1: Total number of signal events expected in data as predicted by MC and observed number of signal events.

4.2 Cross Section

The cross section of central diffraction in data is found using the following relation:

$$\sigma_{\text{data}} = \frac{N_{\text{signal, data}}}{N_{\text{signal, MC}}} \cdot \sigma_{\text{MC}} \tag{4.1}$$

These results are for the parameter space of proton $\xi > 0.02$ and reconstructed mass from **??**, $m > 250$ GeV.

We calculate this separately for both the SaS and ABMST MC:

$$\sigma_{\text{data, SaS}} = (0.063 \pm 0.002\ (\text{stat}) \pm 0.007\ (\text{syst -}))\ \text{mb}$$
$$\sigma_{\text{data, ABMST}} = (0.055 \pm 0.002\ (\text{stat}) \pm 0.006\ (\text{syst}))\ \text{mb}$$

Given that SaS is used as the default, we allow $\sigma_{\text{data, SaS}}$ to be the nominal and use the cross section found from ABMST as another theory uncertainty. Then the cross section we find is:

$$\sigma_{\text{data}} = (0.063 \pm 0.002\ (\text{stat}) \pm 0.007\ (\text{syst})) \pm 0.008\ (\text{theory}))\ \text{mb}$$

For visualization, we can plot this against the predicted cross sections by the models we test (Figure 4.1), with the error on the data being the quadrature sum of each associated uncertainty.

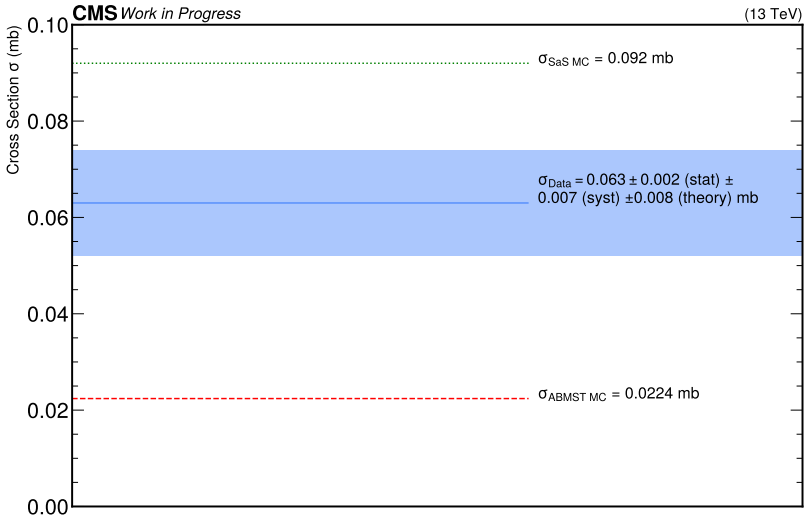

Figure 4.1: Cross section of data, SaS MC, and ABMST MC for proton $\xi > 0.02$ and $m > 250$ GeV.

4.3 Comparison of Data and Monte Carlo Distributions

We plot stacked of the signal taken from MC and background taken from the sideband subtracted background in the SR, and plot the total data in the SR.

SaS Monte Carlo

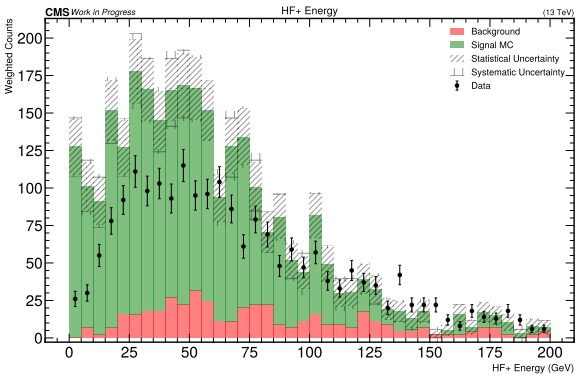

(a) HF Plus Energy

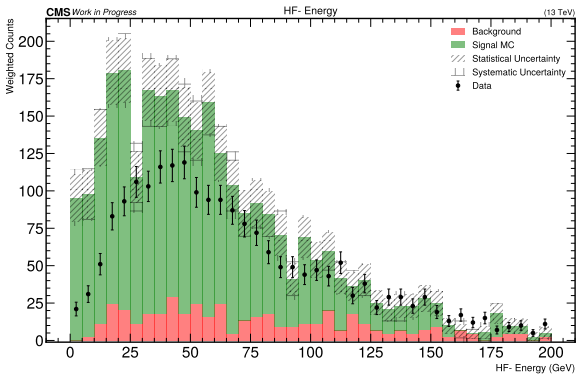

(b) HF Minus Energy

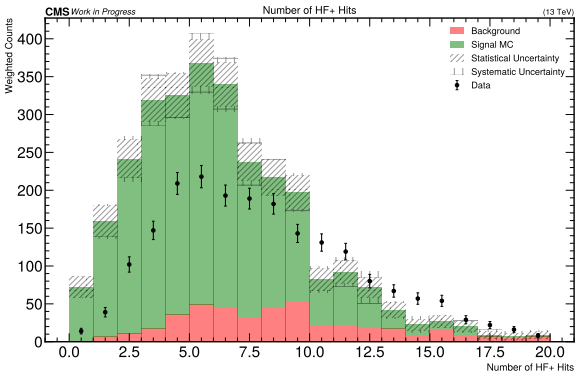

(c) Number of HF Plus Hits

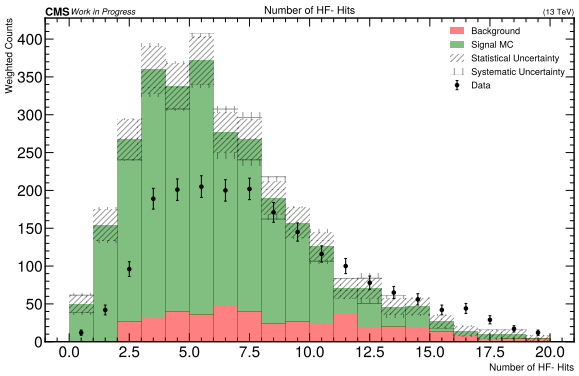

(d) Number of HF Minus Hits

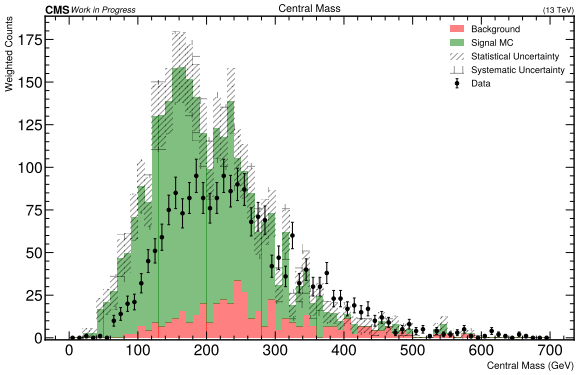

(e) PF Central Mass

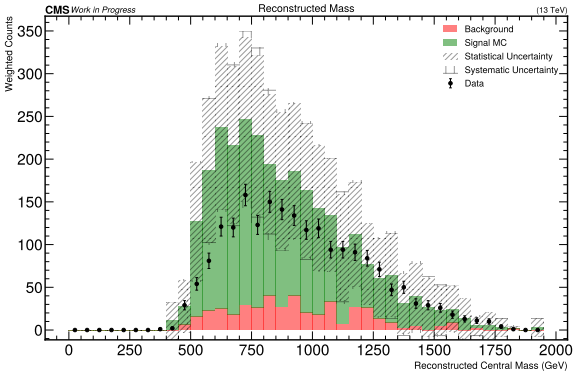

(f) Reconstructed Central Mass

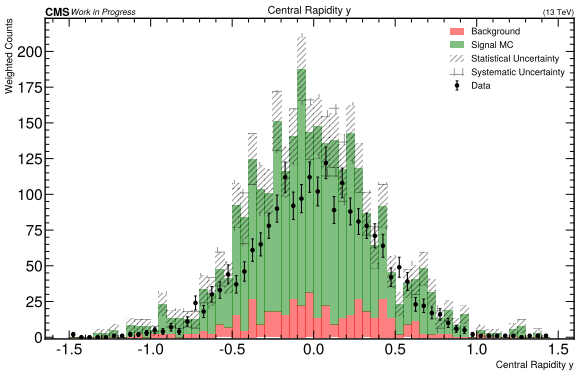

(g) PF Central Rapidity

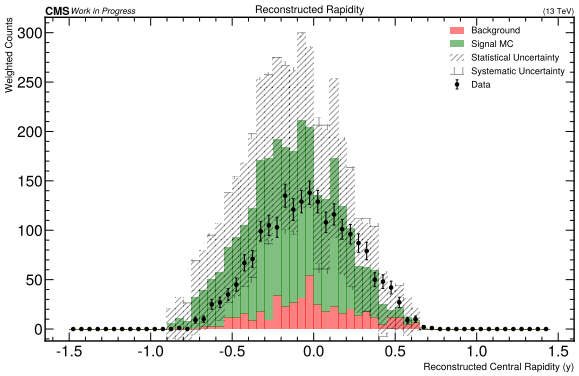

(h) Reconstructed Central Rapidity

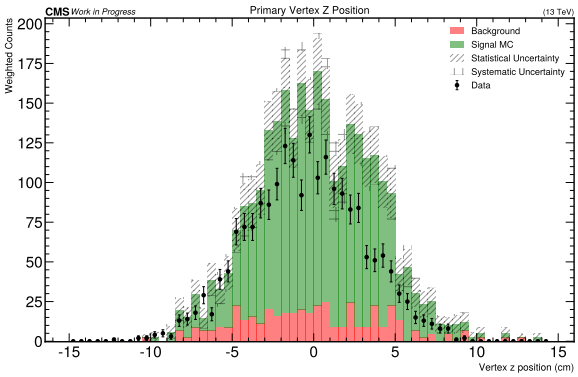

(i) Primary Vertex Z Position

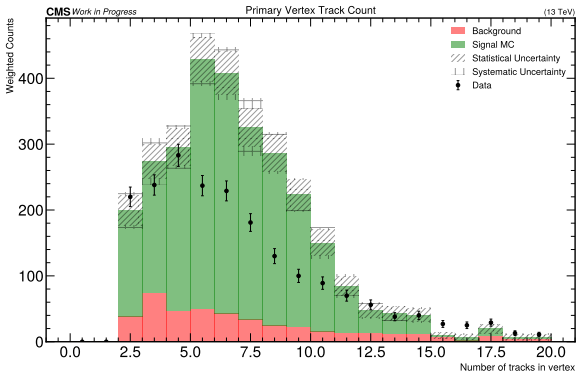

(j) Primary Vertex Number of Tracks

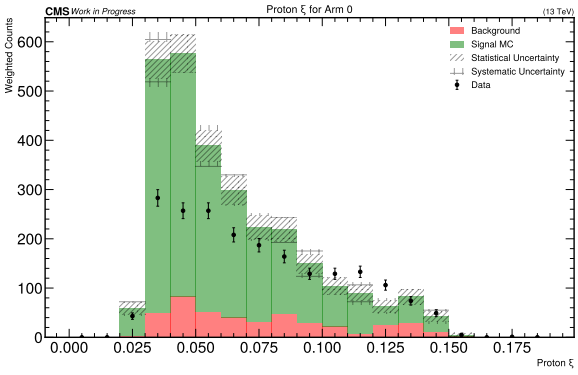

(k) Proton ξ Arm 1

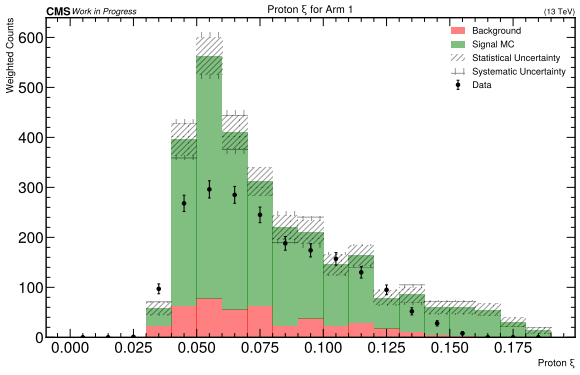

(l) Proton ξ Arm 1

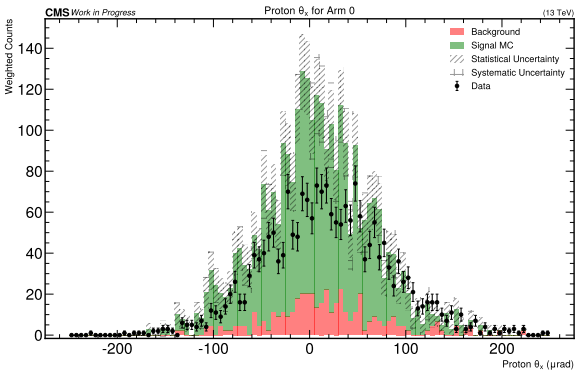

(m) Proton θ_x Arm 0

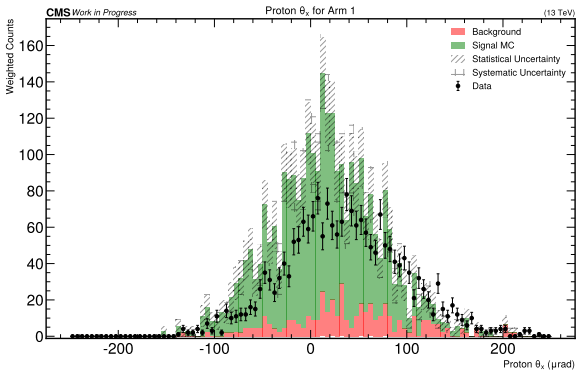

(n) Proton θ_x Arm 1

Figure 4.1: Comparison of data and SaS MC signal and sideband subtracted background distributions.

ABMST Monte Carlo

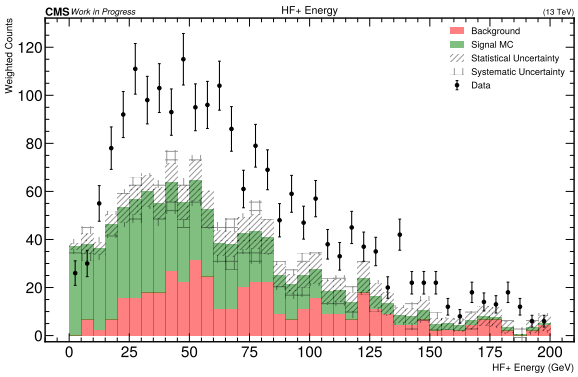

(a) HF Plus Energy

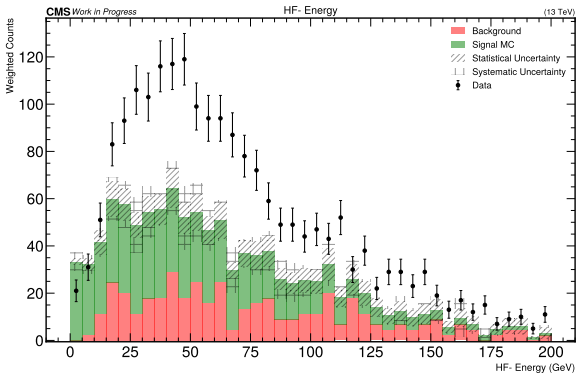

(b) HF Minus Energy

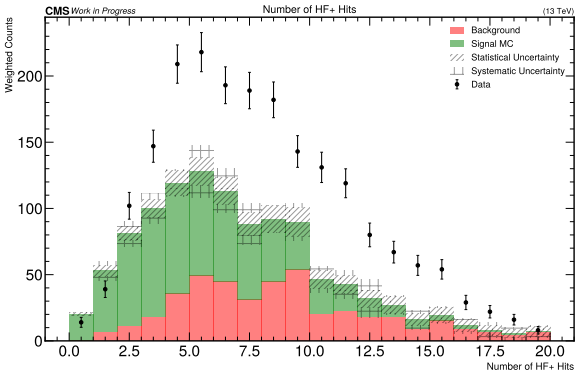

(c) Number of HF Plus Hits

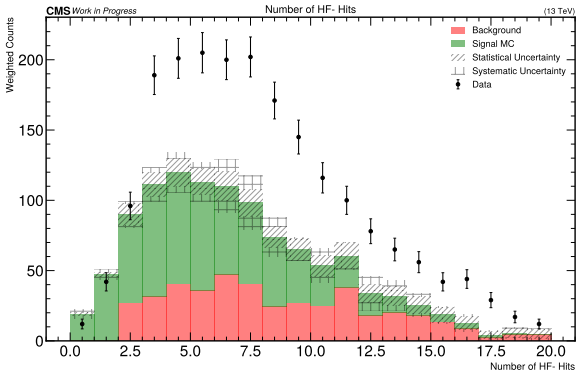

(d) Number of HF Minus Hits

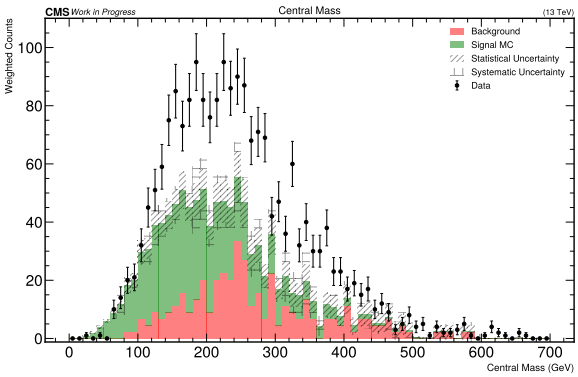

(e) PF Central Mass

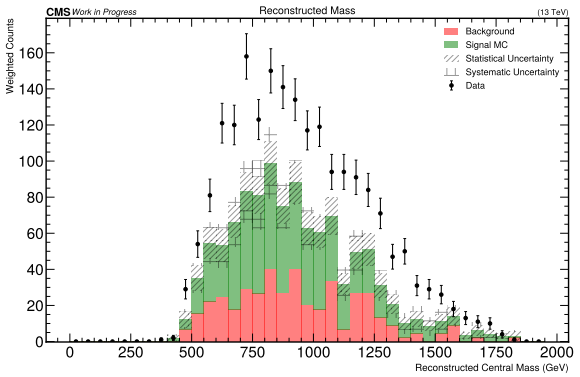

(f) Reconstructed Central Mass

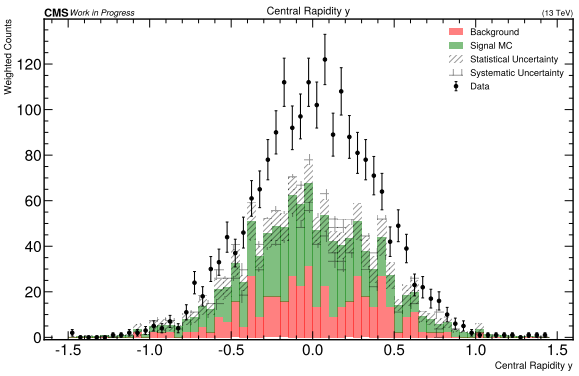

(g) PF Central Rapidity

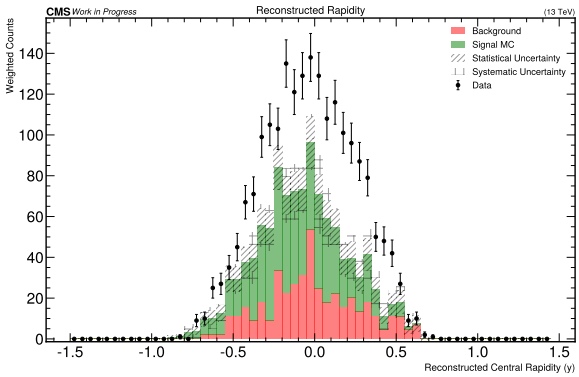

(h) Reconstructed Central Mass

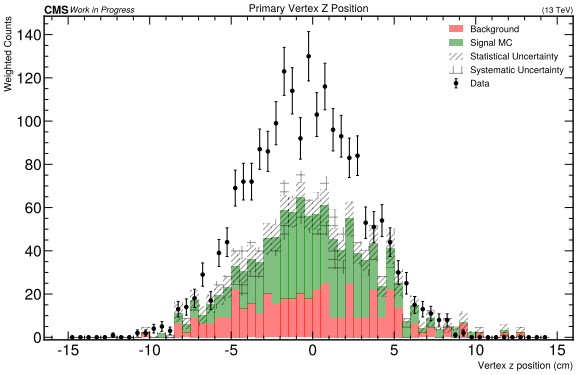

(i) Primary Vertex Z Position

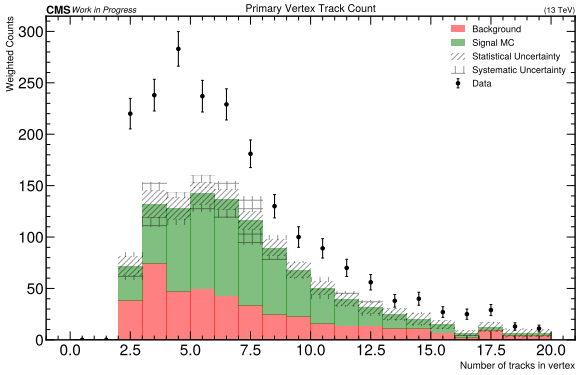

(j) Primary Vertex Number of Tracks

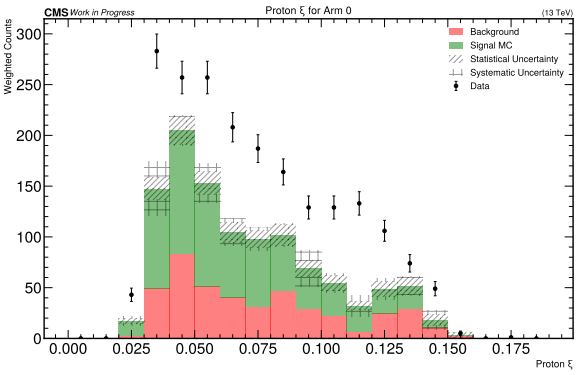

(k) Proton ξ Arm 1

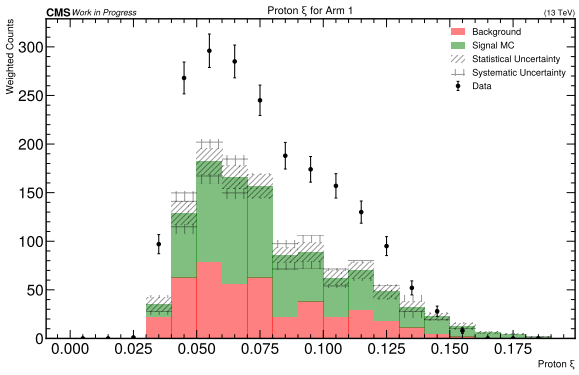

(l) Proton ξ Arm 1

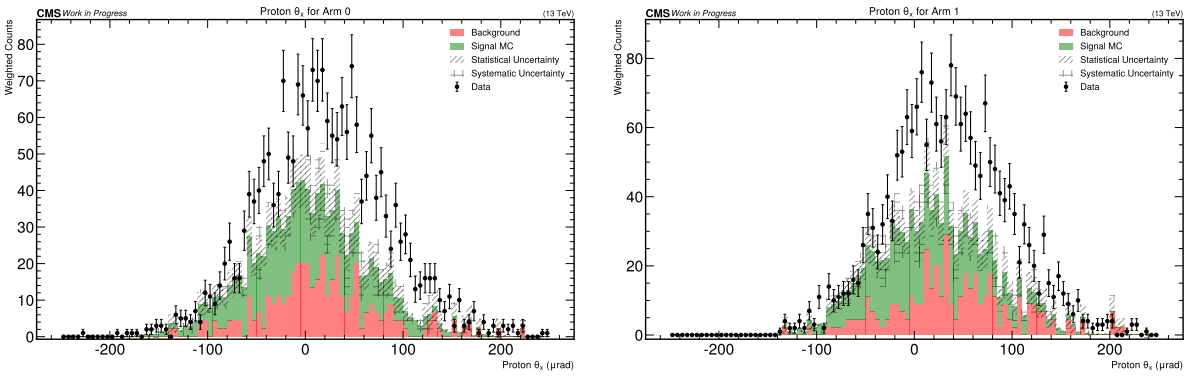

(m) Proton θ_x Arm 0

(n) Proton θ_x Arm 1

Figure 4.2: Comparison of data and ABMST MC signal and sideband subtracted background distributions.

5 Testing High Luminosity Upgrades of the Precision Proton Spectrometer

In preparation for the High Luminosity LHC (HL-LHC), new timing detectors for PPS are being developed and tested. This upgrade will replace the current diamond sensors with low gain avalanche diode (LGAD) detectors. To evaluate their performance, we were allocated one week of beam time at the H6 test beam area in CERN's Prévessin site at the end of August, following a week of preparation. The primary goal of this test beam was to study sensors irradiated earlier in May.

The preparatory work focused on characterizing the amplifiers used in the experimental setup. Because LGAD signals must first be amplified, it was essential to understand amplifier response to signal, noise, crosstalk, and S-parameters to isolate amplification effects. Each measurement was repeated for different amplifier supply voltages. Typically, voltages were varied in 0.5–1 V steps from 0 V up to $V_{\text{max}} - 1$ Vand then in 0.1 V steps from $V_{\text{max}} - 1$ V to V_{max}. For most amplifiers, the maximum operational voltage was 5 V. Given the large number of amplifiers and the repetitive measurements required, I automated the process with simple, reusable scripts to make future characterization faster and more efficient.

The first automation script performed voltage sweeps. I implemented a class to connect to a power supply, and another to execute voltage sweeps, designed to interface easily with other measurement scripts.

Intrinsic noise was measured by monitoring the amplifier output on an oscilloscope without any input signal. To measure signal response, a generator provided an input signal emulating LGAD output, with 1 kHz frequency, 12 ns pulse width, 1.5 V amplitude, 2.5 ns rise/fall times, and negative polarity. A 40 dB attenuator was used to prevent amplifier saturation. We first measured the attenuator response, then the amplifier response. For multi-channel boards, adjacent channels were also monitored to quantify crosstalk. This process was automated with an oscilloscope class that interfaced with the voltage supply class, allowing us to store 1000 waveforms per voltage setting. S-parameter measurements were carried out with a vector network analyzer (VNA), focusing on S_{21} and S (input reflection and gain). A de-embedding procedure was first performed by measuring all four S-parameters over the frequency range of interest, using the SOLT calibration method. Amplifier measurements were then taken for the S-parameters of

interest for frequencies to 1.5 GHz. Because the VNA could only acquire a limited number of samples per range, I wrote another script to enable more flexible data-taking at arbitrary frequencies and resolutions.

6 Conclusion

We measured the fiducial cross section of central diffraction in data to be $\sigma_{\text{data}} = (0.063 \pm 0.002\ (\text{stat}) \pm 0.007\ (\text{syst})) \pm 0.008\ (\text{theory}))$ mb. The SaS model predicts a cross section of 0.092 mb, while the ABMST model predicts 0.0224 mb. Both model predictions disagree with our measurement.

The overall shapes of the distributions predicted by both MC simulations generally agree with data, with some variations. These are most apparent in the SaS MC and likely result from statistical variations.

In future iterations of this study, simulating the SaS MC sample with more statistics may improve the measurement. Further future prospects may include testing some of the other models of central diffraction, incorporating more data samples into the analysis, and further optimizing the event selection beyond the simple cuts-based method used in this analysis.

References

[1] V. Khachatryan and H. Heath. 'Measurement of diffraction dissociation cross sections in pp collisions at s = 7 TeV'. English. In: *Physical Review A: Atomic, Molecular and Optical Physics* D92.1 (2015), p. 012003. ISSN: 1050-2947. DOI: 10.1103/PhysRevD.92.012003.

[2] C. O. Rasmussen and T. Sjöstrand. 'Models for total, elastic and diffractive cross sections'. In: *The European Physical Journal C* 78.6 (June 2018). ISSN: 1434-6052. DOI: 10.1140/epjc/s10052-018-5940-8. URL: http://dx.doi.org/10.1140/epjc/s10052-018-5940-8.

[3] *Proton reconstruction with the CMS Precision Proton Spectrometer in Run 2*. Tech. rep. Geneva: CERN, 2022. URL: https://cds.cern.ch/record/2803842.

[4] M. Albrow et al. *CMS-TOTEM Precision Proton Spectrometer*. Tech. rep. 2014. URL: https://cds.cern.ch/record/1753795.

[5] A. Tumasyan et al. 'Proton reconstruction with the CMS-TOTEM Precision Proton Spectrometer'. In: *JINST* 18.09 (2023), P09009. DOI: 10.1088/1748-0221/18/09/P09009. arXiv: 2210.05854 [hep-ex].

[6] *Sideband Subtraction - CMS Open Data Guide — cms-opendata-guide.web.cern.ch*. https://cms-opendata-guide.web.cern.ch/analysis/selection/idefficiencystudy/tutorial/03-sidebandsubtraction/. [Accessed 26-08-2025].

Appendices

A Event Selection

Zero Time Removal

Without the removal of times equal to 0 there is far greater noise in the data.

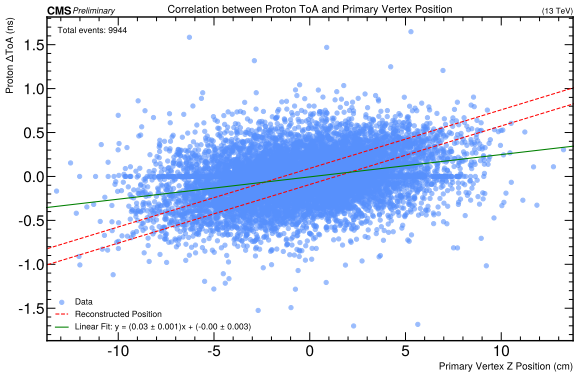

(a) Time correlation, no zero time removal

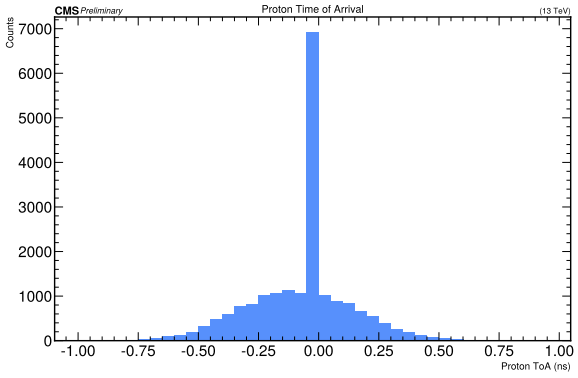

(b) Proton time, no zero time removal

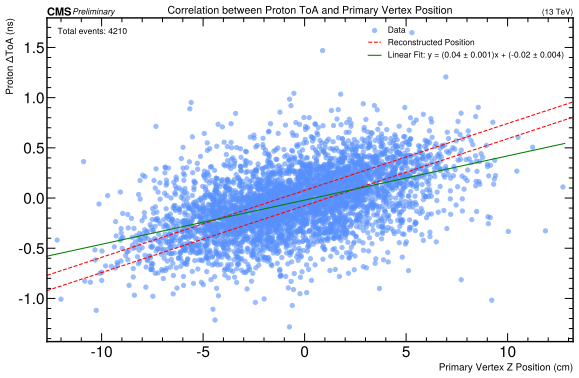

(c) Time correlation, with zero time removal

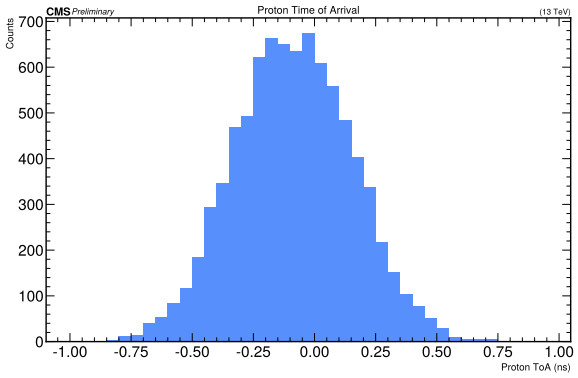

(d) Proton time, with zero time removal

Figure A.1: Time correlation and proton time histogram with baseline cuts and with/without zero time removal.

Baseline Cut Distribution Comparisons

For MC, the SaS MC is used for comparison.

Cut-flow Table

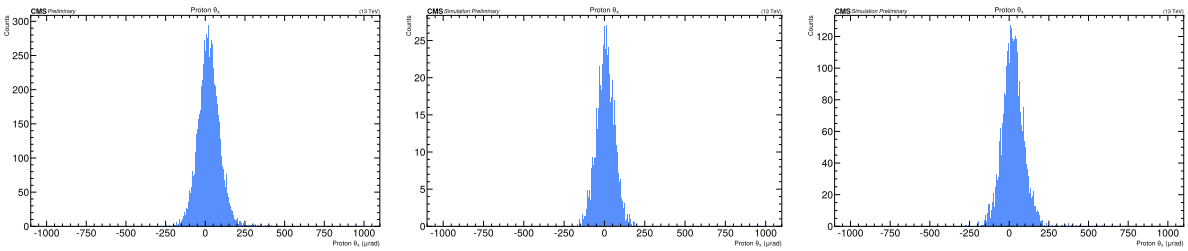

(a) Data (b) MC (c) Event mixing

Figure A.2: ProtonThX distributions after baseline cuts.

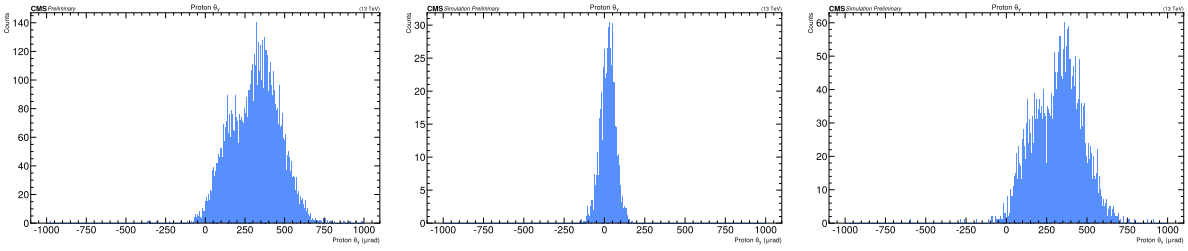

(a) Data (b) MC (c) Event mixing

Figure A.3: ProtonThY distributions after baseline cuts.

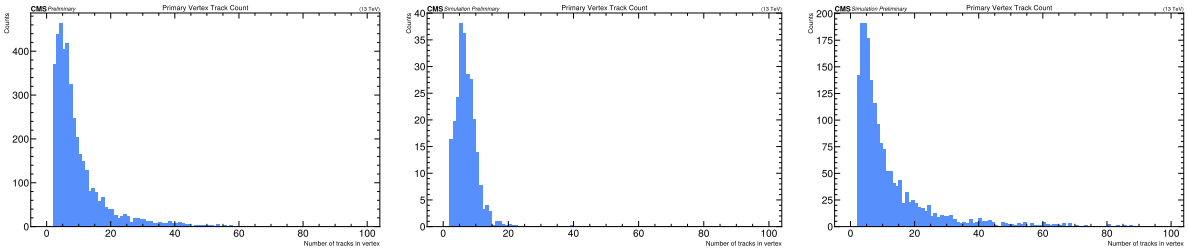

(a) Data (b) MC (c) Event mixing

Figure A.4: PrimVertexNtrk distributions after baseline cuts.

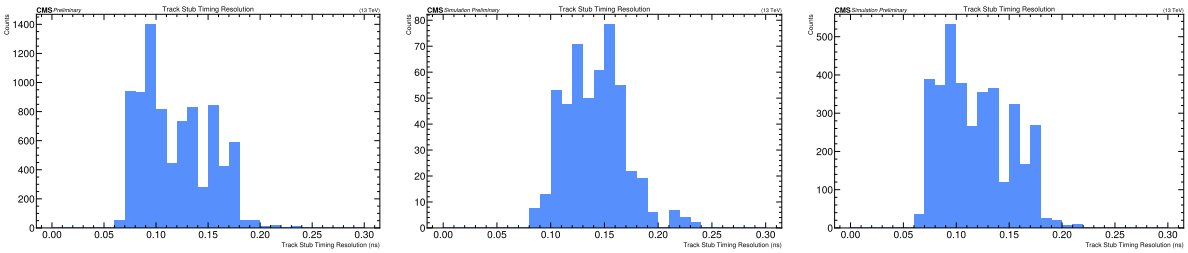

(a) Data (b) MC (c) Event mixing

Figure A.5: TimingTrackTErr distributions after baseline cuts.

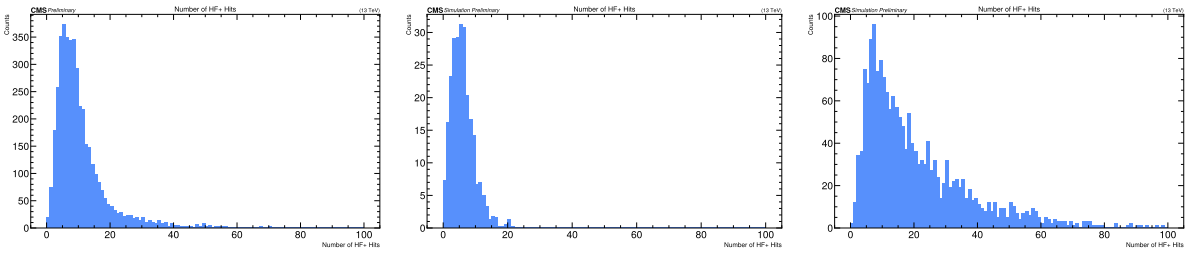

(a) Data (b) MC (c) Event mixing

Figure A.6: nHFplus distributions after baseline cuts.

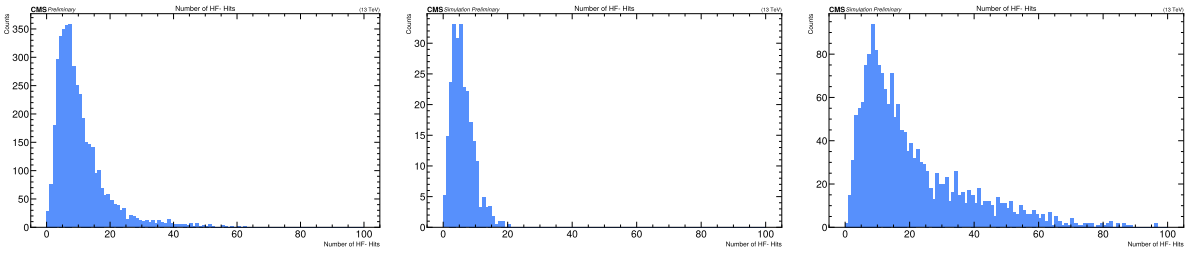

(a) Data (b) MC (c) Event mixing

Figure A.7: nHFminus distributions after baseline cuts.

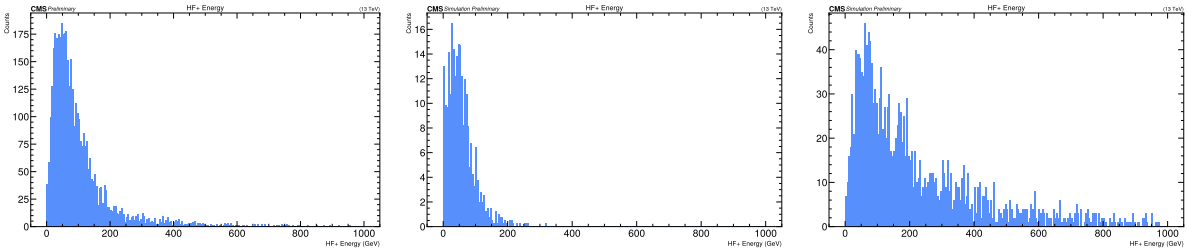

(a) Data (b) MC (c) Event mixing

Figure A.8: HFplusE distributions after baseline cuts.

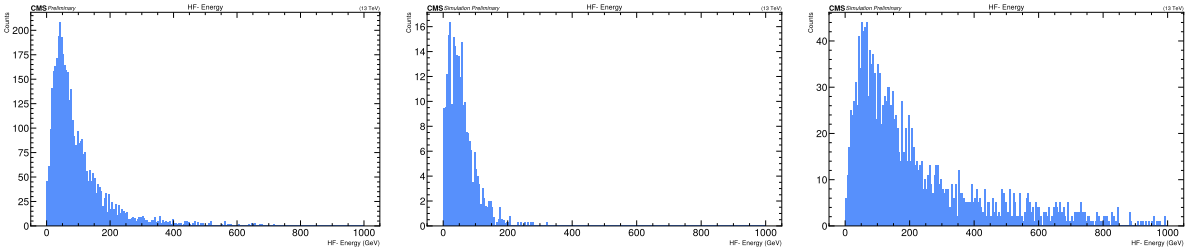

(a) Data (b) MC (c) Event mixing

Figure A.9: HFminusE distributions after baseline cuts.

Cut	Data	SaS MC	ABMST MC	Event-mixing
2 MultiRP protons	103884	2499	39598	100000
1 Vertex	33840	2422	38206	100000
2 Timing tracks	9944	993	14452	100000
Proton timing	5187	993	14452	26853
Proton ThX	5144	993	14452	26562
Proton ThY	4128	993	14452	21516
Vertex Ntrk	3749	990	14429	18331
Timing track error	3749	941	13622	18232
Proton arm selection	3007	941	13622	8430
nHF plus	2890	941	13596	5293
nHf minus	2768	941	13579	4222
HF plus	2714	931	13476	3988
HF minus	2661	920	13337	3788
Timing track arm	2661	920	13337	559

Table A.1: Event cut flow for data, MC and event mixing skimming after applying cuts in Table 2.1.